Chaotic dynamics of the magnetic field generated by dynamo action in a turbulent flow

2008 J. Phys.: Condens. Matter 20 494203

(http://iopscience.iop.org/0953-8984/20/49/494203)

J. Phys.: Condens. Matter **20** (2008) 494203 (6pp) doi:10.1088/0953-8984/20/49/494203

Chaotic dynamics of the magnetic field generated by dynamo action in a turbulent flow

F Pétrélis and S Fauve

Laboratoire de Physique Statistique, CNRS UMR 8550, Ecole Normale Supérieure, 24 rue Lhomond, F-75005 Paris, France

E-mail: petrelis@lps.ens.fr

Received 8 August 2008, in final form 29 September 2008
Published 12 November 2008
Online at stacks.iop.org/JPhysCM/20/494203

Abstract

We present models related to the results of a recent experiment (the 'VKS experiment') showing the generation of a magnetic field by a fully turbulent flow of liquid sodium. We first discuss the geometry of the mean magnetic field when the two coaxial impellers driving the flow counter-rotate at the same frequency. We then show how we expect this geometry to be modified when the impellers rotate at different frequencies. We also show that, in the latter case, dynamical regimes of the magnetic field can be easily understood from the interaction of modes with dipolar (respectively quadrupolar) symmetry. In particular, this interaction generates magnetic field reversals that have been observed in the experiment and display a hierarchy of timescales similar to the Earth's magnetic field: the duration of the steady phases is widely distributed, but is always much longer than the time needed to switch polarity. In addition to reversals, several other large scale features of the generated magnetic field are obtained when varying the governing parameters of the flow. These results are also understood in the framework of the same model.

(Some figures in this article are in colour only in the electronic version)

1. Introduction: the dynamo effect

It is strongly believed that planetary and stellar magnetic fields are generated by a dynamo effect, i.e. an instability mechanism that results from electromagnetic induction by the flow of an electrically conducting fluid [1]. Maxwell's equations together with Ohm's law give the governing equation of the magnetic field, $\mathbf{B}(\mathbf{r}, t)$. In the approximation of magnetohydrodynamics (MHD), it takes the form

$$\frac{\partial \mathbf{B}}{\partial t} = \nabla \times (\mathbf{V} \times \mathbf{B}) + \frac{1}{\mu_0 \sigma} \nabla^2 \mathbf{B}, \tag{1}$$

where μ_0 is the magnetic permeability of vacuum and σ is the electrical conductivity. The last term on the right-hand side of (1) represents ohmic dissipation, and the first one, electromagnetic induction due to the velocity field $\mathbf{V}(\mathbf{r}, t)$. $B = 0$ is an obvious solution of (1) and, for $V = 0$, any perturbation of $\mathbf{B}(\mathbf{r}, t)$ (respectively of current density $\mathbf{j}(\mathbf{r}, t)$) decays to zero due to ohmic diffusion. $B = 0$ can be an unstable solution if the induction term compensates ohmic dissipation. The ratio of these two terms defines the magnetic Reynolds number, $R_m = \mu_0 \sigma V L$, where V is the typical velocity amplitude and L is the typical length scale of the flow. If $\mathbf{V}(\mathbf{r}, t)$ has an appropriate geometry, perturbations of the magnetic field grow when R_m becomes larger than a critical value R_m^c (in the range 10–1000 for most studied examples). Magnetic energy is generated from part of the mechanical work used to drive the flow.

In order to describe the saturation of the magnetic field above the dynamo threshold R_m^c, we need to take into account its backreaction on the velocity field. $\mathbf{V}(\mathbf{r}, t)$ is governed by the Navier–Stokes equation:

$$\frac{\partial \mathbf{V}}{\partial t} + (\mathbf{V} \cdot \nabla)\mathbf{V} = -\nabla \left(\frac{p}{\rho} + \frac{B^2}{2\mu_0 \rho} \right) + \nu \nabla^2 \mathbf{V} + \frac{1}{\mu_0 \rho} (\mathbf{B} \cdot \nabla)\mathbf{B}, \tag{2}$$

that we have restricted to the case of an incompressible flow ($\nabla \cdot \mathbf{V} = 0$). ν is the kinematic viscosity and ρ is the fluid density. In the MHD approximation, the Lorenz force,

$\mathbf{j} \times \mathbf{B}$, can be split into the two terms involving $\mathbf{B}$ in (2). If the modification of the flow under the action of the growing magnetic field weakens the dynamo capability of the flow, the dynamo bifurcation is supercritical, i.e. the magnetic field grows continuously from zero when R_m is increased above R_m^c.

Assuming that the set of parameters defined so far fully characterizes the problem, we should have another independent dimensionless parameter besides R_m. We can choose either the kinetic Reynolds number, $Re = VL/\nu$, or the magnetic Prandtl number, $P_\mathrm{m} = R_\mathrm{m}/Re = \mu_0\sigma\nu$. Then, dimensional analysis implies that we have $R_\mathrm{m}^c = f(P_\mathrm{m})$ for the dynamo threshold and $\langle B^2\rangle = \mu_0\rho V^2 g(R_\mathrm{m}, P_\mathrm{m})$ for the mean magnetic energy generated above the dynamo threshold. f and g are arbitrary functions at this stage. Their dependence on P_m (or equivalently on Re) can be related to the effect of turbulence on the dynamo threshold and saturation. In many realistic situations, more parameters should be taken into account. For instance, f and g also depend on the choice of boundary conditions (for instance, their electrical conductivity, magnetic permeability, etc). In the context of stellar or planetary dynamos, the effect of the rotation rate Ω should also be taken into account via the Rossby, $Ro = V/\Omega L$, or Ekmann number $E = \nu/\Omega L^2$.

For planetary or stellar dynamos, as well as for any laboratory experiment performed with a liquid metal, we have $Pm < 10^{-5}$, the largest value being reached using liquid sodium. This has strong consequences on the dynamo bifurcation and makes the problem both difficult and interesting. P_m being the ratio of the diffusive timescales of the magnetic field and the velocity field, no direct numerical simulation can handle such small values. In addition, P_m being small implies that the flow is strongly turbulent when the dynamo threshold is reached ($Re \sim R_\mathrm{m}^c/P_\mathrm{m} > 10^6$). Dynamo experiments thus provide a way to study an instability problem from a fully turbulent state. Several interesting questions arise: does the generated magnetic field involve a mean large scale component, as observed in planetary or stellar dynamos? What are the behaviours of f and g when $P_\mathrm{m} \to 0$? Are they constant with respect to P_m in this limit, thus giving $R_\mathrm{m}^c =$ constant and $\langle B^2\rangle \propto \mu_0\rho V^2 g(R_\mathrm{m})$, i.e. $\langle B^2\rangle \propto [\rho/(\mu_0\sigma^2 L^2)]g(R_\mathrm{m})$ close to threshold [2]? What is the effect of turbulent fluctuations on the bifurcation? Is $g(R_\mathrm{m}) \propto R_\mathrm{m} - R_\mathrm{m}^c$, as for a usual supercritical bifurcation close to threshold, or should we expect a behaviour involving an anomalous exponent [3]? What is the effect of turbulent fluctuations on the dynamics of the magnetic field?

2. The VKS experiment

The velocity field being turbulent above the dynamo threshold for any experiment performed with a liquid metal, we can use the Reynolds decomposition and write $\mathbf{V}(\mathbf{r}, t) = \overline{\mathbf{V}}(\mathbf{r}) + \tilde{\mathbf{v}}(\mathbf{r}, t)$, where $\overline{\mathbf{V}}(\mathbf{r})$ is the mean flow and $\tilde{\mathbf{v}}(\mathbf{r}, t)$ are the turbulent fluctuations. The overbar stands for a temporal average in experiments. Thus, both the mean flow $\overline{\mathbf{V}}(\mathbf{r})$ and the fluctuations $\tilde{\mathbf{v}}(\mathbf{r}, t)$ are involved in the induction term of (1) and one has to understand their respective effects on the dynamo process.

Three successful fluid dynamo experiments have been performed so far: the Karlsruhe experiment [4], the Riga experiment [5] and the VKS experiment [6]. The VKS experiment differs from the other two as follows: the Karlsruhe and Riga experiments have been designed by geometrically constraining a mean flow $\overline{\mathbf{V}}(\mathbf{r})$ known for its efficient dynamo action, the G O Roberts flow (respectively the Ponomarenko flow) for the Karlsruhe (respectively Riga) experiment. Turbulent fluctuations, roughly an order of magnitude smaller than the mean flow, have been discarded, and the experimentally observed dynamo threshold as well as the geometry of the mean magnetic field have been found in good agreement with these predictions, based only on the mean flow.

The VKS experiment consists of a von Kármán swirling flow of liquid sodium. It is generated in a cylinder by the motion of two coaxial counter-rotating discs fitted with eight blades (see figure 1). The mean flow has the following characteristics: the fluid is ejected radially outward by the discs; this drives an axial flow toward the discs along their axis and a recirculation in the opposite direction along the cylinder lateral boundary. In the case of counter-rotating impellers, the presence of a strong axial shear of azimuthal velocity in the mid-plane between the impellers generates a high level of turbulent fluctuations, roughly of the same order as the mean flow. It is thus unlikely that the fluctuations $\tilde{\mathbf{v}}$ can be neglected compared to $\overline{\mathbf{V}}$ in (1). It has been indeed observed that, when the discs counter-rotate with the same frequency, $F_1 = F_2$, a stationary magnetic field is generated with a dominant axial dipolar component, $\mathbf{B}_P$, together with a related azimuthal component $\mathbf{B}_\theta$, as displayed in figure 1 (left) [6]. Such an axisymmetric mean field cannot be generated by the mean flow alone, $\overline{\mathbf{V}}(r, x)$, which would give a non-axisymmetric magnetic field according to the Cowling theorem [1], and also as observed in numerical modelling performed using $\overline{\mathbf{V}}(r, x)$ alone [7]. Non-axisymmetric fluctuations $\tilde{\mathbf{v}}(r, \theta, x)$ thus play an essential role. As explained in [3], a possible mechanism is of α–ω type, the α effect being related to the helical motion of the radially expelled fluid between two successive blades of the impellers and the ω effect resulting from differential rotation due to counter-rotation of the impellers. However, any quantitative model of this effect should also take into account the helicity of radial vortices generated by the shear flow in the mid-plane that has the wrong sign to generate an axial mean field from an α–ω mechanism.

Another possibility is an α^2 mechanism for which the mean field equation is very easy to find using symmetry arguments. If one assumes that a closed equation exists for the mean field $\mathbf{B}_0$, the mean induction term is, to leading order, $\mathcal{E} = \langle \mathbf{V} \times \mathbf{B}\rangle \simeq M \cdot \mathbf{B}_0$, where M is a 3×3 matrix. Rotational invariance about the rotation axis implies $\mathcal{E} = a\mathbf{B}_0 - b\hat{\mathbf{x}} \times \mathbf{B}_0 + c(\hat{\mathbf{x}} \cdot \mathbf{B}_0)\hat{\mathbf{x}}$, where a, b and c can depend weakly on x and $\hat{\mathbf{x}}$ is the unit vector along the rotation axis. In the case of counter-rotating discs at the same frequency, the experiment is invariant with respect to a rotation of π around any axis located in the mid-plane between the two discs, say $\mathcal{R}_\pi$. This implies $b = 0$ and shows that the equations for the components $B_r(r, x, t)$ and $B_x(r, x, t)$ of the mean field

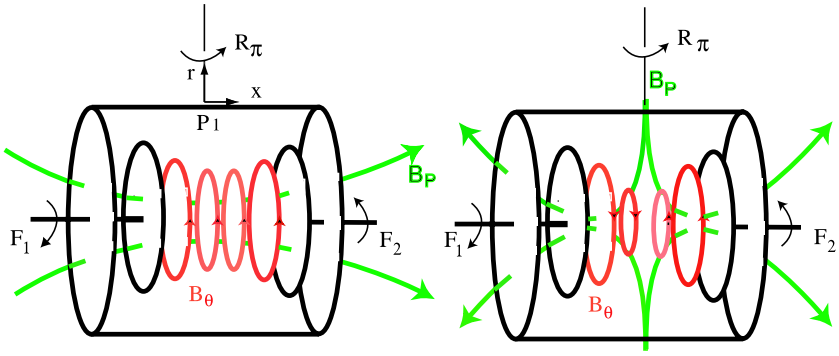

Figure 1. Possible eigenmodes of the VKS experiment. The two discs counter-rotate with frequency F_1 and F_2. Left: magnetic dipolar mode. Right: magnetic quadrupolar mode. Poloidal ($\mathbf{B}_P$) and toroidal ($\mathbf{B}_\theta$) components are sketched.

are qualitatively different when the discs rotate at different frequencies (see below).

In any case, the VKS dynamo is not generated by the mean flow alone, in contrast to the Karlsruhe and Riga experiments, and non-axisymmetric fluctuations play an essential role in the dynamo process. Note also that the VKS dynamo has been observed so far only when impellers made of soft iron have been used. Indeed, it has been shown that magnetic boundary conditions corresponding to the high permeability limit significantly decrease the dynamo threshold [8].

3. Dynamics resulting from the interaction of dipolar and quadrupolar modes

3.1. Modes and symmetries

The most striking feature of the VKS experiment is that time-dependent magnetic fields are generated only when the impellers rotate at different frequencies [9]. We will show that this can be related to the additional invariance under $\mathcal{R}_\pi$ when $F_1 = F_2$. We indeed expect that, in that case, the modes involved in the dynamics are either symmetric or antisymmetric. Such modes are displayed in figure 1. A dipole is changed to its opposite by $\mathcal{R}_\pi$, whereas a quadrupole is unchanged. More generally, we name 'dipole' (respectively 'quadrupole') modes with dipolar (respectively quadrupolar) symmetry even though they might involve a more complex spatial structure.

We assume that the magnetic field is the sum of a dipolar component with an amplitude D and a quadrupolar one, Q. We define $A = D + \mathrm{i}Q$ and we assume that an expansion in power of A and its complex conjugate $\bar{A}$ is pertinent close to threshold in order to obtain an evolution equation for both modes. Taking into account the invariance $\mathbf{B} \to -\mathbf{B}$, i.e. $A \to -A$, we obtain

$$\dot{A} = \mu A + \nu \bar{A} + \beta_1 A^3 + \beta_2 A^2 \bar{A} + \beta_3 A \bar{A}^2 + \beta_4 \bar{A}^3, \quad (3)$$

where we limit the expansion to the lowest order nonlinearities. In the general case, the coefficients are complex and depend on the experimental parameters.

Symmetry of the experiment with respect to $\mathcal{R}_\pi$ when the discs exactly counter-rotate amounts to constraints on the coefficients. Applying this transformation to the magnetic modes changes D into $-D$ and Q into Q, and thus $A \to -\bar{A}$. We conclude that, in the case of exact counter-rotation, all the coefficients are real. When the frequency difference f is increased from zero, assuming that the coefficients are analytical functions of f, we obtain that the real parts of the coefficients are even and the imaginary parts are odd functions of f.

When the coefficients are real, the growth rate of the dipolar component is $\mu_r + \nu_r$ and that of the quadrupolar component is $\mu_r - \nu_r$. The dipole being observed for exact counter-rotation implies that $\nu_r > 0$ for $f = 0$. By increasing f, we expect that ν_r changes sign and favours the quadrupolar mode according to the experimental results (see figure 3 in [10]).

We point out that equation (3) looks like the normal forms for strong resonances, i.e. for the complex amplitude of an oscillatory mode generated by a Hopf bifurcation in the presence of an external forcing. The $\bar{A}$ (respectively $\bar{A}^3$) term results from a forcing around twice (respectively 4 times) the frequency of the oscillatory instability (see [11] for a study of the bifurcations and resulting dynamics).

We note that a model involving coupled dipolar and quadrupolar modes that bifurcate through Hopf bifurcations instead of stationary ones, as considered here, has been proposed to understand some features of the dynamics of the magnetic field of the Sun [12].

3.2. A simple case

We first consider the simplest case for which the nonlinear terms which break rotational invariance in the complex plane are negligible ($\beta_{1r} \sim \beta_{3r} \sim \beta_{4r} \sim 0$) and we assume $\beta_{2r} = -1$ to ensure nonlinear saturation. We write

$$A = D + \mathrm{i}Q = R \exp(\mathrm{i}(\theta + \theta_0)), \quad (4)$$

with θ_0 such that $\nu \exp(-2\mathrm{i}\theta_0) = \rho$ is real. The imaginary part of the equation for $\dot{A}$ then gives

$$\dot{\theta} = \mu_i - \rho \sin 2\theta. \quad (5)$$

When the flow is perfectly symmetric, i.e. when the two impellers rotate at the same frequency, $\mu_i = 0$. Then for $\mu_r + \nu_r > 0$, the system has two stable dipolar solutions

(corresponding to both polarities). For $0 < \mu_r - \nu_r < \mu_r + \nu_r$, two quadrupolar modes are also solutions, but they are unstable to a dipolar perturbation. When the symmetry of the flow is broken, μ_i is different from zero and this can strongly modify the behaviour of the solutions of the above equation. For μ_i smaller than ρ, four solutions exist: θ_c and $\pi + \theta_c$ are stable solutions while $\pi/2 - \theta_c$ and $3\pi/2 - \theta_c$ are unstable ($2\theta_c = \arcsin(\mu_i/\rho)$). They correspond to mixed modes, which evolve away from the purely dipolar modes, with increasing quadrupolar contribution when μ_i is increased. For $\mu_i = \rho$, a bifurcation occurs: each stable solution collides with an unstable solution and disappears. This is a saddle-node bifurcation [11] that generates a limit cycle (and thus an oscillatory magnetic field) for $\mu_i > \rho$. Usually, saddle-node bifurcations involve only one stable and one unstable fixed point. Here the problem being invariant under $\mathbf{B} \to -\mathbf{B}$ yields the existence of two pairs of stable and unstable fixed points that simultaneously collide at the threshold of the saddle-node bifurcation. This scenario is not restricted to the equation for θ that we have considered here (see below).

We have thus found a simple mechanism to explain how the dipolar modes, observed for counter-rotating impellers at the same frequency $F_1 = F_2$ in the VKS experiment first evolve to stationary solutions that also involve a larger and larger quadrupolar component when the frequency difference $|F_1 - F_2|$ is increased. Then, for a critical value of $|F_1 - F_2|$, a limit cycle is generated at finite amplitude and vanishing frequency by a saddle-node bifurcation.

3.3. A generic bifurcation

More generally, consider a planar system invariant under the transformation $\mathbf{B} \to -\mathbf{B}$ and with two different and nonzero stationary solutions. One of the fixed points is unstable, $\mathbf{B}_u$, and the other one is stable, $\mathbf{B}_s$. The collision between the two fixed points generates a cycle that connects the collision point with its opposite, see figure 2. This result can be understood as follows: the solution $B = 0$ is unstable with respect to the two different fixed points, and their opposite. It is an unstable point, whereas one of the two bifurcating solutions is a stable point, a node, and the other is a saddle. If the saddle and the node collide, say at B_c, what happens to initial conditions located close to these points? They cannot be attracted by $B = 0$ which is unstable and they cannot reach other fixed points since they just disappeared. Therefore the trajectories describe a cycle. The associated orbit contains $B = 0$ since, for a planar problem, in any orbit, there is a fixed point. Suppose that the orbit created from B_c is different from the one created by $-B_c$. These orbits being images by the transformation $\mathbf{B} \to -\mathbf{B}$, they must intersect at some point. Of course, this is not possible for a planar system because it would violate the uniqueness of the solutions. Therefore, there is only one cycle that connects points close to B_c and $-B_c$.

This provides an elementary mechanism for field reversals in the vicinity of a saddle-node bifurcation. First, in the absence of fluctuations, the limit cycle generated at the saddle-node bifurcation connects $\pm B_c$. This corresponds to periodic reversals. Slightly above the bifurcation threshold, the system spends most of the time close to the two states of opposite polarity $\pm B_c$. Second, in the presence of fluctuations, random reversals can be obtained slightly below the saddle-node bifurcation. $\mathbf{B}_u$ being very close to $\mathbf{B}_s$, even a fluctuation of small intensity can drive the system to $\mathbf{B}_u$ from which it can be attracted by $-\mathbf{B}_s$, thus generating a reversal.

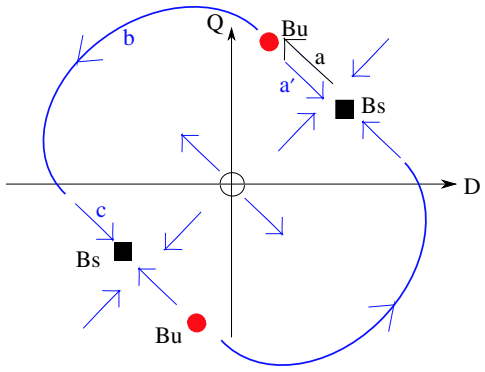

Figure 2. A generic saddle-node bifurcation in a system with the $\mathbf{B} \to -\mathbf{B}$ invariance: below threshold, fluctuations can drive the system against its deterministic dynamics (phase a). If the effect of fluctuations is large enough, this generates a reversal (phases b and c). Otherwise, an excursion occurs (phase a′).

3.4. Different stationary dynamos

It has been observed in the VKS experiment that, for $F_1 \neq F_2$, dynamical regimes are separated by domains with different stationary dynamos in parameter space [9, 10]. In our model, these stationary dynamos correspond to fixed points of equation (3). Taking into account the term $\bar{A}^3$ instead of $\bar{A}$ and repeating the simple analysis of section 3.2 shows that the saddle-node bifurcation involves four pairs of fixed points due to the invariance $A \to A\exp(\mathrm{i}\pi/2)$. More generally, when all terms of (3) are taken into account, we can have two pairs of different fixed points together with the ones of opposite polarity, as observed in the experiment [10]. Their stability analysis is easy in the regime of phase dynamics, i.e. when the amplitude R involves a short timescale compared to the phase θ. This occurs when μ_r is large compared to μ_i, ν_r and ν_i and R then can be adiabatically eliminated ($R \simeq R_0(\theta)$), (3), thus leading to an equation of the form $\dot{\theta} = G(\theta)$. When the parameters are varied, the different pairs of fixed points disappear via successive saddle-node bifurcations as described above. There is a region in parameter space (F_1, F_2) where the two saddle-node bifurcations occur nearly simultaneously. Turbulent fluctuations then generate complex dynamical regimes in which the different fixed points are involved (see below).

3.5. Effect of fluctuations

We now use a simple model in order to describe the effect of turbulent fluctuations on the dynamics of the two magnetic

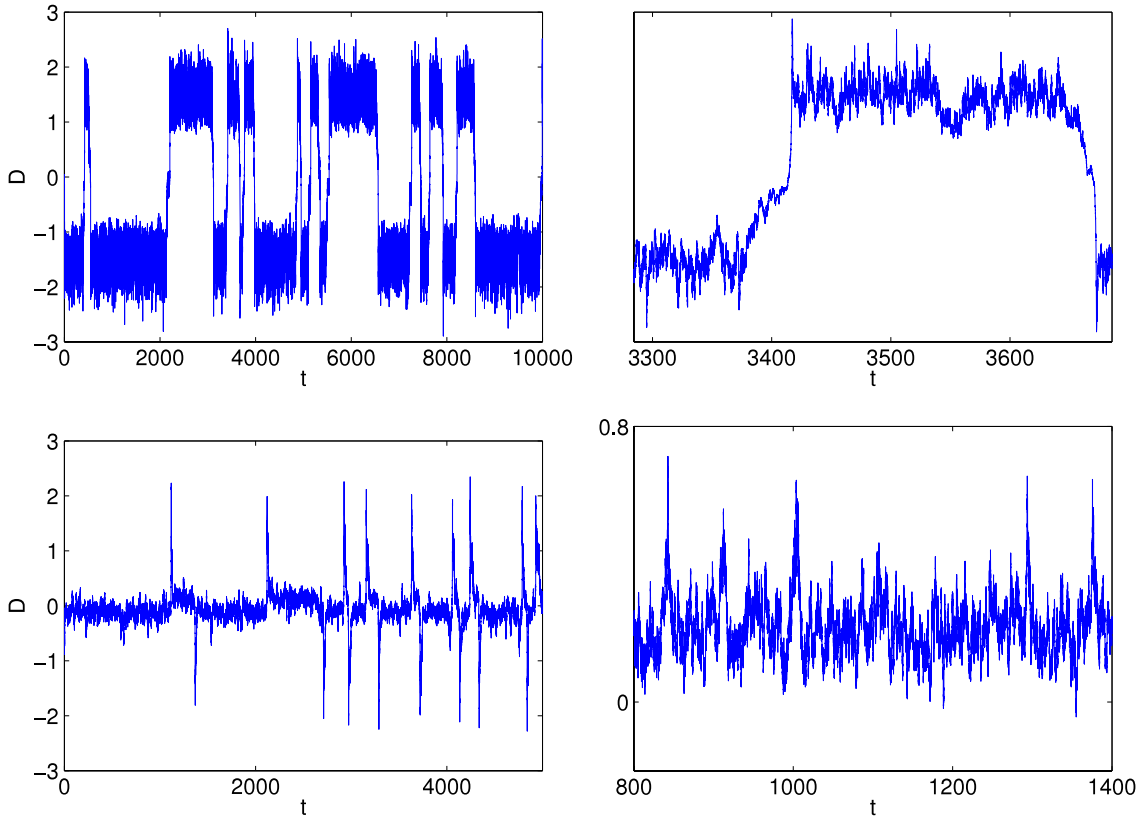

Figure 3. Time recordings obtained from equation (3) displaying different dynamics of the magnetic field, as observed in the VKS experiment: reversals, symmetric bursts and asymmetric bursts (see the text).

modes governed by (3):

$$\begin{aligned}\dot{D} &= (\mu_r + \nu_r)D + (\nu_i - \mu_i)Q + C_{11}D^3 + C_{21}D^2Q \\ &\quad + C_{31}DQ^2 + C_{41}Q^3 + br_1\zeta_1(t)D + br_2\zeta_2(t)Q, \\ \dot{Q} &= (\mu_r - \nu_r)Q + (\nu_i + \mu_i)D + C_{12}D^3 + C_{22}D^2Q \\ &\quad + C_{32}DQ^2 + C_{42}Q^3 + br_3\zeta_3(t)D + br_4\zeta_4(t)Q.\end{aligned} \tag{6}$$

The nonlinear coefficients C_{ij} are derived from those of equations (3). Turbulent fluctuations are modelled by the terms ζ_i that are independent Gaussian white noises (with the Stratonovich interpretation). We take $\mu_r = 1$ and $\nu_r = \mu_i = \nu_i = 0$ such that phase dynamics results from the nonlinear terms. We take $\beta_{2r} = -1$, $\beta_{1r} = \beta_{3r} = 0$, $\beta_{1i} - \beta_{3i} = -0.9$, $\beta_{2i} = -\beta_{4i} = 0.12$. We vary $\beta_{1i} + \beta_{3i}$ and β_{4r} in order to favour one or the other pair of fixed points. We take $br_1 = br_4 = 0.25$ and $br_2 = br_3 = 0.07$.

Random reversals are displayed in figure 3 (top) for $\beta_{1i} + \beta_{3i} = -0.021$ and $\beta_{4r} = -0.06$. For these parameters, the low amplitude pairs of fixed points have just disappeared via a saddle-node bifurcation. The system spends most of the time close to the stable fixed points $\pm B_s$. We observe in figure 3 (top right) that a reversal consists of two phases. In the first phase, the system evolves from the stable point B_s to the unstable point B_u (in the phase space sketched in figure 2). The deterministic part of the dynamics acts against this evolution and the fluctuations are the motor of the dynamics. That phase is thus slow. In the second phase, the system evolves from B_u to $-B_s$, the deterministic part of the dynamics drives the system and this phase is faster.

The behaviour of the system close to B_s depends on the local flow. Close to the saddle-node bifurcation, the position of B_s and B_u defines the slow direction of the dynamics. If a component of B_u is smaller than the corresponding one of B_s, that component displays an overshoot at the end of a reversal. In the opposite case, that component will increase at the beginning of a reversal. For instance, in the phase space sketched in figure 2, the component D decreases at the end of a reversal and the signal displays an overshoot. The component Q increases just before a reversal.

For some fluctuations, the second phase does not connect B_u to $-B_s$ but to B_s. It is an aborted reversal or an excursion in the context of the Earth dynamo. Note that, during the initial phase, a reversal and an excursion are identical. In the second phase, the approaches to the stationary phase differ because the trajectory that links B_u and B_s is different from the trajectory that links B_u and $-B_s$. In particular, if the reversals display an overshoot this will not be the case of the excursion (see figure 3 (top right) and the sketch in figure 2).

If we choose the parameters such that the large amplitude pairs of fixed points have just disappeared via a saddle-node bifurcation instead of the small amplitude ones as above, we obtain symmetric bursts displayed in figure 3 (bottom left) for $\beta_{1i} + \beta_{3i} = 0.025$ and $\beta_{4r} = 0.03$. From this regime, if we favour further the low amplitude fixed points ($\beta_{1i} + \beta_{3i} = 0.01$

and $\beta_{4r} = 0.06$), we get asymmetric bursts displayed in figure 3 (bottom right). All these regimes have also been observed in the VKS experiment [10].

4. Conclusion

We have proposed a scenario for reversals of the magnetic field generated by dynamo action in the VKS experiment. When the impellers are counter-rotated at different frequencies, the flow breaks the invariance by rotation $\mathcal{R}_\pi$, and thus couples modes with dipolar and quadrupolar symmetries. This coupling drives the system close to a saddle-node bifurcation, such that even non-coherent turbulent fluctuations can generate a reversal. The scenario offers a simple and unified explanation for reversals of a vector field. In particular, it explains many intriguing features of the reversals of the Earth's magnetic field [13]. In that case, dipolar and quadrupolar modes are coupled when the flow in the core breaks the equatorial symmetry. The most significant output of the model is that it predicts specific characteristics observed both in the VKS experiment as well as in palaeomagnetic records. It also explains recent numerical simulations of the geodynamo that have pointed out the importance of hydrodynamic symmetry breaking during reversals [14, 15].

Finally, we note that two modes with the same symmetry can be linearly coupled by a symmetric flow and display the saddle-node bifurcation mentioned above. Nevertheless, when dipolar and quadrupolar magnetic modes are involved, reversals are favoured by breaking the discrete symmetry from which these modes are defined.

Our model also provides an alternative description of oscillatory dynamos, in contrast to Parker's mechanism for the solar cycle that involves a Hopf bifurcation.

References

[1] Moffatt H K 1978 *Magnetic Field Generation in Electrically Conducting Fluids* (Cambridge: Cambridge University Press)
[2] Pétrélis F and Fauve S 2001 *Eur. Phys. J.* B **22** 273
[3] Pétrélis F, Mordant N and Fauve S 2007 *Geophys. Astrophys. Fluid Dyn.* **101** 289
[4] Stieglitz R and Müller U 2001 *Phys. Fluids* **13** 561
[5] Gailitis A, Lielausis O, Platacis E, Dement'ev S, Cifersons A, Gerbeth G, Gundrum T, Stefani F, Christen M and Will G 2001 *Phys. Rev. Lett.* **86** 3024
[6] Monchaux R, Berhanu M, Bourgoin M, Moulin M, Odier Ph, Pinton J-F, Volk R, Fauve S, Mordant N, Pétrélis F, Chiffaudel A, Daviaud F, Dubrulle B, Gasquet C and Marié L 2007 *Phys. Rev. Lett.* **98** 044502
[7] Marié L, Burgente J, Daviaud F and Léorat J 2003 *Eur. Phys. J.* B **33** 469
Bourgoin M, Odier P, Pinton J F and Ricard Y 2004 *Phys. Fluids* **16** 2529
Ravelet F, Chiffaudel A, Daviaud F and Léorat J 2005 *Phys. Fluids* **17** 117104
[8] Gissinger C, Iskakov A, Fauve S and Dormy E 2008 *Europhys. Lett.* **82** 29001
[9] Berhanu M, Monchaux R, Fauve S, Mordant N, Pétrélis F, Chiffaudel A, Daviaud F, Dubrulle B, Marié L, Ravelet F, Bourgoin M, Odier Ph, Pinton J-F and Volk R 2007 *Europhys. Lett.* **77** 59001
[10] Ravelet F, Berhanu M, Monchaux R, Aumaître S, Chiffaudel A, Daviaud F, Dubrulle B, Bourgoin M, Odier Ph, Pinton J-F, Plihon N, Volk R, Fauve S, Mordant N and Pétrélis F 2008 *Phys. Rev. Lett.* **101** 074502
[11] Arnold V 1982 *Geometrical Methods in the Theory of Ordinary Differential Equations* (Berlin: Springer)
[12] Knobloch E and Landsberg A S 1996 *Mon. Not. R. Astron. Soc.* **278** 294
[13] Pétrélis F, Fauve S, Dormy E and Valet J P 2008 Breaking equatorial symmetry favors reversals of the Earth magnetic field arXiv:0806.3756
[14] Li J, Sato T and Kageyama A 2002 *Science* **295** 1887
[15] Nishikawa N and Kusano K 2008 *Phys. Plasmas* **15** 082903